Current Topics

Attenuated Total Reflection Fourier Transform Infrared Spectroscopy: A Method of Choice for Studying Membrane Proteins and Lipids†

Suren A. Tatulian*

Biomolecular Science Center and Department of Molecular Biology and Microbiology, University of Central Florida, Orlando, Florida 32826

Received February 10, 2003; Revised Manuscript Received August 13, 2003

Membrane proteins constitute roughly one-third of all gene products and play key roles in cell function. Despite this, they are poorly represented in the list of proteins with determined atomic-resolution structures, because both crystallography and NMR still encounter difficulties in handling membrane proteins. Large hydrophobic patches of membrane proteins strongly interfere with their crystallization for diffraction experiments (*1*−*3*); only a few examples can be mentioned when the structures of membrane-reconstituted proteins were determined by X-ray crystallography (*3*−*8*). Despite the considerable progress in determining atomic-resolution structures of membrane proteins by solid-state and multidimensional heteronuclear NMR techniques (*9*−*12*), modern macromolecular NMR is limited to particles of moderate size. This prohibits the use of lipid vesicles and forces the investigators to use either organic solvents or detergent micelles to mimic the hydrophobic membrane environment. Clearly, none of the media conventionally used in crystallography or NMR (i.e., crystals, micelles, or organic solvents) feasibly model the properties of the membrane−water interface, the native environment of membrane proteins. Moreover, the correspondence between structural models deduced from crystallography or NMR and the native structure of membrane proteins remains an open question (*13*, *14*). The unique properties of the membrane−water interface indeed determine the structure of membrane proteins in many ways (*15*−*17*). Therefore, development of biophysical techniques for determining the structure and function of membrane proteins under physiological conditions is one of the most demanding problems of modern structural biology. This article highlights recent advances in understanding the structure of membrane proteins and their interactions with lipids by attenuated total reflection Fourier transform infrared (ATR-FTIR)[1] spectroscopy. Some useful features and theoretical aspects of ATR-FTIR spectroscopy of proteins have been reported in previous reviews (*18*−*26*). Our focus is on new developments in biophysical applications of ATR-FTIR spectroscopy, including physical characterization of supported lipid monolayers and bilayers, quantitative description of protein−lipid interactions and accompanying structural effects, protein−protein interactions in membranes, analysis of the mechanisms of membrane-binding enzymes, and advances in isotope-edited and time-resolved difference FTIR spectroscopy. Adequate experimental and data analysis procedures are described, and precaution measures that should be exercised to avoid misinterpretation of the data are outlined.

Analysis of Protein−Lipid Systems by ATR-FTIR Spectroscopy

In an ATR-FTIR experiment, an internal reflection plate (e.g., germanium or ZnSe) is covered with lipid layer(s) containing reconstituted protein(s), and the infrared beam is focused into the plate. The light travels inside the plate by means of a series of internal reflections from one surface of the plate to the other, creating an exponentially decaying evanescent radiation outside the plate. Absorption of the energy of the evanescent field by the supported membrane and the reconstituted protein provides ATR-FTIR spectra that contain a wealth of information about the structure of the system. Because the decay length of the evanescent wave (typically ∼0.2−0.6 μm) extends far beyond the dimensions of largest proteins, there are no concerns regarding the size of the protein. On the other hand, because of large wavelengths of infrared light, light scattering problems are no longer bothersome like in circular dichroism or fluorescence experiments in the UV region. By using polarized light in ATR-FTIR measurements, one evaluates the orientation of the protein with respect to membrane lipids, which is usually not obtained by high-resolution techniques.

The spectra of a protein−lipid system comprise well-resolved absorbance bands not only of both membrane lipids and proteins but also of different structural (or functional) groups of these molecules, without the requirement of labeling. Among various "amide vibrational modes" gener-

† This work was supported by National Institutes of Health Grant HL65524.

* To whom correspondence should be addressed. Phone: (407) 882-2260. Fax: (407) 384-2062. E-mail: statulia@mail.ucf.edu.

[1] Abbreviations: ATR, attenuated total reflection; BR, bacteriorhodopsin; DHPC, dihexadecylphosphatidylcholine; DMPC, dimyristoylphosphatidylcholine; DPG, dipalmitoylglycerol; DPPC, dipalmitoylphosphatidylcholine; DPPG, dipalmitoylphosphatidylglycerol; FTIR, Fourier transform infrared; HX, hydrogen exchange; KcsA, *Streptomyces lividans* K^+ channel; LB, Langmuir−Blodgett; PLA_2, phospholipase A_2; PLB, phospholamban; PLPC, 1-palmitoyl-2-linoleoylphosphatidylcholine; POPC, 1-palmitoyl-2-oleoylphosphatidylcholine; SR, sarcoplasmic reticulum.

10.1021/bi034235+ CCC: $25.00
Published on Web 09/26/2003

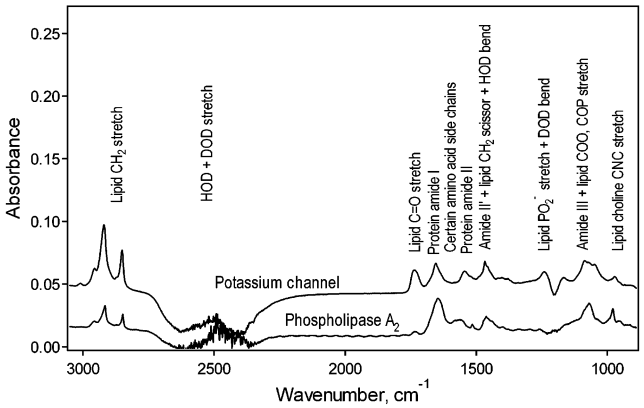

FIGURE 1: ATR-FTIR spectra of phospholipid bilayers supported on a germanium plate with reconstituted *S. lividans* K^+ channel and with a membrane-bound secretory PLA_2, as indicated. The membranes contain POPC (or DPPC) in the lower leaflet and a 4/1 POPC/POPG mixture (or asolectin) in the upper leaflet, for PLA_2 and K^+ channel, respectively. The spectra are recorded at perpendicular polarization of the infrared light, under D_2O buffers containing 100 mM NaCl, 15 mM KCl, 10 mM Hepes, and 2 mM $CaCl_2$ (pD 8.0) for PLA_2 and 150 mM NaCl and 10 mM Tris-HCl (pD 7.4) for K^+ channel.

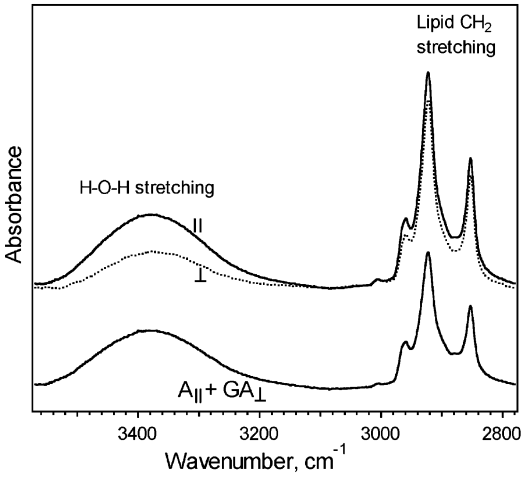

FIGURE 2: The upper two spectra are the ATR-FTIR spectra of a supported POPC monolayer at parallel (—) and perpendicular (···) polarizations of the infrared light. The lower spectrum is a polarization-independent spectrum obtained with $A = A_{||} - 0.422A_{\perp}$.

ated by a polypeptide chain, the amide I mode (~1700−1600 cm^{-1}) is most sensitive to the protein secondary structure, and the amide II mode (~1545 cm^{-1}) is sensitive to the amide hydrogen exchange (HX) kinetics (*20*, *27*−*32*). Two representative ATR-FTIR spectra of supported membranes with an incorporated integral membrane protein, K^+ channel, and with peripherally membrane-bound phospholipae A_2 (PLA_2) are presented in Figure 1. Even the comparison of these panoramic spectra indicates apparent structural differences between the two systems. Distinct line shapes of amide I bands of the K^+ channel and PLA_2 reflect secondary structural features of these proteins. The stronger amide II band of the K^+, channel compared to that of PLA_2, indicates slower HX for the K^+ channel, probably because it is protected from the solvent (D_2O) by the membrane (*33*). The decreased intensity of lipid bands in the case of PLA_2 evidently results from PLA_2-catalyzed lipid hydrolysis and partial dissociation of the reaction products from the membrane (*34*, *35*). More detailed characterization of protein−lipid systems by ATR-FTIR is described in the following sections.

Lipid Monolayers and Bilayers

Lipid bilayer membranes supported on solid substrates have been successfully used as models of cellular membranes (*36*, *37*). A variety of techniques have been devised for preparation of supported membranes, most of which include spreading of vesicles either directly on a solid surface or on a preformed lipid monolayer, with or without an underlying polymer cushion (*33*−*46*). Since the presence of excess water is critical for the structure of both proteins and lipids, samples in the bulk aqueous phase correspond to physiological conditions to a larger extent than those prepared by drying proteoliposomes on the surface of the plate (*21*−*23*, *47*−*51*).

Lipid monolayers are conventionally deposited on the internal reflection plate by the Langmuir−Blodgett (LB) technique (*33*−*35*, *39*−*41*, *52*, *53*). As described below, the lipid packing density and the physical state (e.g., gel or liquid-crystalline), the orientational order parameter, the thickness of the water layer trapped between the membrane and the substrate, and the number of trapped water molecules per lipid can be determined. Two spectra of a POPC monolayer at parallel and perpendicular polarizations of the infrared light (relative to the incidence plane) in the region covering the lipid CH_2 and water HOH stretching bands are shown in Figure 2. The ATR dichroic ratio of the lipid acyl chains (R^{ATR}), i.e., the ratio of the intensities of CH_2 stretching bands at parallel and perpendicular polarizations, equals $A_{||}/A_{\perp}$ (=1.17), and the order parameter is determined by eq 1 of the Supporting Information ($S = 0.05$). ATR order parameters can change in the region between −0.5 and 1, corresponding to orientations of the molecular axis parallel or perpendicular to the membrane plane, respectively, and an order parameter S of 0 corresponds either to an isotropic orientational distribution or to a fixed orientation at 54.7°. An order parameter of 0.05 indicates a large degree of disorder in the acyl chains of POPC, which results from the unsaturated bond in the *sn*-2 chain. The frequencies of CH_2 stretching vibrations are known to increase upon gel-to-liquid crystal phase transitions of lipids. In particular, the asymmetric CH_2 band shifts from ~2916 to ~2924 cm^{-1} upon phase transition (*28*, *54*). For POPC monolayers, this vibrational mode occurs at 2922.8 cm^{-1}, confirming the disordered, fluid-like state of the lipid.

The lipid packing density in the monolayer, Γ, is determined by eq 4 of the Supporting Information, using the following parameters: the measured integrated intensity of the lipid CH_2 band (2990−2812 cm^{-1}), $A_{||} = 1.638$ cm^{-1}, the integrated extinction coefficient of the lipid [$\epsilon_{lipid} = 1.32 \times 10^8$ cm/mol (*55*)], $n_{12} = 4/1.43$, $N = 42$, $\gamma = 45°$, $E_x = 1.411$, and $E_z = 0.738$ (for an explanation, see the Supporting Information). This yields a Γ of 2.3×10^{-10} mol/cm^2, which corresponds to a cross-sectional area per POPC molecule of 72 Å^2.

The absorbance of polarized light by spatially oriented molecules depends on the molecular orientation. Therefore, for determination of the molar ratio of two differently oriented components in the system, one needs a spectrum

Table 1: Parameters Characterizing the Structure and Hydration of Lipid Monolayers As Determined by ATR-FTIR Spectroscopy[a]

lipid	$A_{lipid,\|\|}$ (cm^{-1})	$A_{lipid,\perp}$ (cm^{-1})	S	ν_{as,CH_2} (cm^{-1})	a_{lipid} ($Å^2$)	A_{water} (cm^{-1})	W/L	h (Å)
DPG	3.20	2.88	0.23	2916.5	35.7	0.69	3.8	3.2
DHPC	2.72	2.52	0.33	2917.1	44.8	0.84	5.9	3.9
DPPC	2.13	2.15	0.70	2919.5	49.9	0.81	7.2	4.3
DMPC	1.71	1.57	0.30	2921.7	58.1	1.02	9.3	4.8
POPC	1.64	1.40	0.05	2922.8	72.0	1.39	14.8	6.2
PLPC	1.51	1.26	−0.03	2924.4	75.5	1.44	16.0	6.3

[a] All absorbances are the integrated areas of corresponding bands, hence the dimension cm^{-1}. For water, an extinction coefficient ϵ_{water} of 1.17×10^7 cm/mol was used (from ref *56*). Extinction coefficients for lipids were found by correcting that of POPC [1.32×10^8 cm/mol (*55*)], using the numbers of CH_2 groups in the hydrocarbon chains of each lipid, as described in the text.

which is not affected by polarization. "Polarization-independent" spectra can be obtained using two spectra measured at parallel and perpendicular polarizations [$A = A_{||} + GA_{\perp}$, where $G = (2E_z^2 - E_x^2)/E_y^2$ (*25*), and E_x, E_y, and E_z are the orthogonal electric vector components of the evanescent field in the membrane (see ref *25* and the Supporting Information)]. Such a spectrum was obtained for the POPC monolayer using a scaling factor for a Ge-deposited thin film under air, where $G = -0.422$ (lower part of Figure 2). This spectrum was used to find the ratio of absorbance intensities of the trapped water and the lipid [$A_{water}/A_{lipid} = 1.312$ (the intensity of the water band was integrated in the region of 3540−3200 cm^{-1})]. This ratio was used in eq 5 of the Supporting Information along with integrated extinction coefficients of the lipid and water [$\epsilon_{water} = 1.17 \times 10^7$ cm/mol (*56*)] to determine the water/lipid molar ratio (=14.8). The spacing between the lipid monolayer and the plate is estimated by multiplying the number of waters per lipid (14.8) by the molecular volume of water (29.92 $Å^3$) and dividing by the cross-sectional area per lipid (72 $Å^2$), which yields an h of ≈6.2 Å.

Data for monolayers of various lipids (Table 1) indicate that the lipid order parameter decreases upon incorporation of one or two unsaturated bonds in the acyl chains (POPC and PLPC, respectively) and significantly increases upon elongation of acyl chains (compare DMPC and DPPC). For ester phospholipids (DPPC, DMPC, POPC, and PLPC), there is an inverse proportionality between the lipid order parameters and CH_2 stretching frequencies. For all six lipids, tighter lipid packing densities correspond to lower CH_2 stretching frequencies and to fewer water molecules per lipid.

Supported lipid bilayers can be prepared by injecting lipid vesicles into the cell, containing the plate covered with a monolayer; interaction of vesicles with the hydrophobic surface causes spreading and formation of supported bilayers (*33*−*35*, *39*, *40*, *52*, *53*). Direct spreading of sonicated vesicles on Ge plates also produces high-quality supported bilayers, especially if the vesicles contain acidic lipids and the buffer includes ≥1 mM $CaCl_2$ (*34*). Comparison of the spectra of a DPPC monolayer with the spectra of a DPPC/asolectin bilayer indicated the appearance of the olefinic CH stretching band at ∼3010 cm^{-1}, broadening of the methylene bands, a blue shift of their frequencies, and a decrease in the packing order in the bilayer compared to the monolayer, resulting from the highly unsaturated hydrocarbon chains in asolectin (*33*). This was confirmed by a decrease in the order parameter S from ≈0.7 (monolayer) to 0.42 (bilayer). These data demonstrate that supported lipid monolayers and bilayers can be comprehensively characterized by ATR-FTIR, and physical properties of the membranes can be regulated by changing their lipid composition.

Membrane Binding of Peripheral and Integral Proteins

Supported membranes are well suited for studying both peripheral and integral membrane proteins. The solution of a peripheral protein can be directly injected into the ATR cell, followed by adsorption of the protein to the membrane (*34*, *35*, *41*, *52*). In the case of integral proteins, vesicles with incorporated protein(s) are allowed to spread on the monolayer and to yield bilayers with the reconstituted protein (*33*, *39*, *40*, *53*).

The protein-to-lipid molar ratio (P/L) can be determined from a "polarization-independent" spectrum, which can be obtained using a G of ≈0.8 for a Ge-supported thin membrane in aqueous buffer. The P/L ratio is calculated with eq 5 of the Supporting Information, using integrated intensities of the lipid CH_2 stretching band and the protein amide I band, corrected for corresponding extinction coefficients. The extinction coefficient of the lipid CH_2 band can be determined from the spectra of quantitatively deposited monolayers, or by using an ϵ_{POPC} of 1.32×10^8 cm/mol (*55*), corrected for the number of CH_2 groups in the hydrocarbon chains of the lipid (n_{CH_2}); i.e., $\epsilon_{lipid} = n_{CH_2} \times 1.32 \times 10^8/28 = n_{CH_2} \times 4.71 \times 10^6$ cm/mol. The extinction coefficients of protein bands depend on the secondary structure. Venyaminov and Kalnin (*57*) reported the following integrated extinction coefficients per peptide unit: 7.6×10^7, 0.5×10^7, 7.0×10^7, and 4.5×10^7 cm/mol for α-helix, for the high- and low-frequency components of β-sheet, and for irregular ("random") structures, respectively. For a given protein, a weighted average of the extinction coefficient should be obtained on the basis of its secondary structure and multiplied by the number of peptide bonds (n_p) in the protein. For a secretory PLA_2, which incorporates 50% α, 10% β, and 40% irregular structure, a weighted average for $\epsilon_{protein}$ of $n_p \times 5.7 \times 10^7$ cm/mol was obtained (*34*).

The number of protein molecules bound per unit area of the lipid bilayer (n) can be estimated using the P/L molar ratio as (*34*, *35*)

$$n = \frac{P/L}{a_{lipid}/2} \tag{1}$$

where a_{lipid} is the cross-sectional area per lipid. Binding of PLA_2 to supported membranes was described by a Langmuir-type adsorption isotherm supplemented with the Hill cooperativity coefficient

$$n = \frac{NC^{\alpha_H}K^{\alpha_H}}{1 + C^{\alpha_H}K^{\alpha_H}} \tag{2}$$

where N is the number of binding sites per unit area, C is the PLA_2 concentration, K is the apparent binding constant, and α_H is the Hill coefficient. Adsorption isotherms characterizing binding of PLA_2 to supported membranes composed of DPPC/DPPG bilayers at various ionic strengths are presented in Figure 3. The binding parameters (N, K, and α_H) have been evaluated independently using two types of

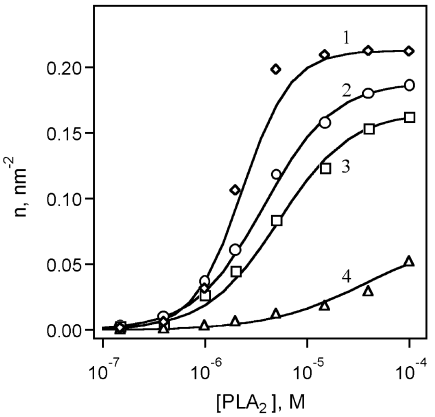

FIGURE 3: Binding of PLA_2 to supported membranes composed of DPPC and DPPG (3/2 molar ratio). The buffer contained 5 mM Tris-HCl, 0.5 mM EGTA, and 1 mM NaN_3 in D_2O (pD 8.2), with 0, 0.01, 0.1, and 1 M NaCl (curves 1−4, respectively). The curves are simulated by eq 2 using the following parameters: $K = 4.3 \times 10^5$ M^{-1}, $N = 0.213$ nm^{-2}, and $\alpha_H = 1.85$ (curve 1), $K = 2.6 \times 10^5$ M^{-1}, $N = 0.189$ nm^{-2}, and $\alpha_H = 1.28$ (curve 2), $K = 1.9 \times 10^5$ M^{-1}, $N = 0.166$ nm^{-2}, and $\alpha_H = 1.24$ (curve 3), and $K = 2.8 \times 10^4$ M^{-1}, $N = 0.07$ nm^{-2}, and $\alpha_H = 0.93$ (curve 4).

Scatchard plots (*34*). The data indicate a significant weakening of the binding of PLA_2 to membranes with increasing ionic strength, which evidently results from the suppression of electrostatic attraction between the cationic PLA_2 molecule and negatively charged membranes.

Reconstitution of integral proteins in supported membranes involves solubilization in detergents and transfer of the protein to lipid vesicle membranes either by incubation with Bio-Beads (such as SM-2) or by dilution with a suspension of vesicles so that the detergent concentration drops below the critical micelle concentration (*33*, *39*, *40*, *53*, *58*). Addition of proteoliposomes to a preformed lipid monolayer results in spreading of the vesicles atop the monolayer and formation of supported membranes with reconstituted integral protein(s). The protein-to-lipid ratio then can be determined as described above. Because the integral proteins span the membrane, the expression for the surface density of the protein now should involve the cross-sectional areas of both the lipid and the protein; i.e., the denominator of eq 1 should be $a_{lipid}/2 + a_{protein}$.

Membrane Protein Structure, Dynamics, and Orientation

The preferred solvent in protein FTIR spectroscopy is D_2O, rather than H_2O, because (i) H_2O strongly absorbs around 1645 cm^{-1} and obscures the protein amide I band, (ii) amide I components of α-helical and irregular structures overlap in the region of 1660−1650 cm^{-1}, and (iii) the use of D_2O allows assessment of the amide HX that contains valuable information about the protein dynamics. Since the irregular structure undergoes HX and shifts to lower frequencies (∼1645 cm^{-1}) much faster (∼1 s) than α-helix does (minutes to hours), spectra measured between exposure to D_2O for several minutes and 1−2 h provide spectrally separated irregular and helical components and therefore contain more information about protein structure than those measured in H_2O or after prolonged exposure to D_2O. Figure 4 presents three pairs of polarized ATR-FTIR spectra in the amide I and amide II regions for the *Streptomyces lividans* K^+ channel (KcsA) reconstituted in a DPPC/asolectin bilayer

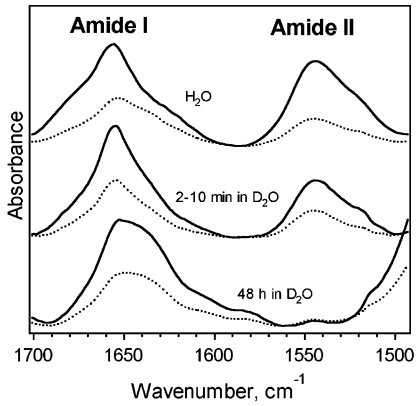

FIGURE 4: Polarized ATR-FTIR spectra of *S. lividans* K^+ channel reconstituted in a supported DPPC/asolectin bilayer in H_2O or D_2O buffer, as indicated. The H_2O buffer contained 150 mM NaCl and 10 mM NaP_i (pH 7.4), and the D_2O buffer contained 150 mM NaCl and 10 mM Tris-HCl (pD 7.4). The solid and dotted lines correspond to parallel and perpendicular polarizations, respectively, of the infrared light.

(*33*). The spectra measured in H_2O and at different times of exposure to D_2O indicate profound changes in both amide I and amide II bands resulting from amide HX. These spectra have been used to describe the secondary and dynamic structures of the protein (*33*).

Amide Hydrogen Exchange and Protein Dynamics. The kinetics of amide HX have been determined by analyzing spectral changes in both amide I and amide II regions (*33*−*35*, *41*, *52*, *53*, *58*). Amide HX results in shifts of both amide I and amide II bands toward lower frequencies by ∼10 and ∼100 cm^{-1}, respectively (from ∼1650 to ∼1640 cm^{-1} and from ∼1545 to ∼1450 cm^{-1}, respectively). The exchanged amide II′ band at ∼1450 cm^{-1} cannot be used for HX analysis because of the overlap with both solvent and lipid vibrational modes (Figure 1). The kinetics of exchange can be measured on the basis of the decrease in the intensity of the unexchanged amide II band at ∼1545 cm^{-1}. The amide II intensity must be normalized by using the ratio of the areas of amide II and amide I bands ($A_{amideII}/A_{amideI}$) to avoid errors related to loss or gain of the membrane-bound protein. If the numbers of unexchanged and exchanged residues in the protein are *H* and *D*, respectively, then the fraction of unexchanged amide protons at a time *t* is defined as the fraction of residual amide II band intensity, which is described by a multiexponential function (*33*)

$$\left(\frac{H}{H+D}\right)_t = \frac{\left(\frac{A_{amideII}}{A_{amideI}}\right)_t}{\left(\frac{A_{amideII}}{A_{amideI}}\right)_0} = \sum_{i=1}^{m} a_i e^{-t/\tau_i} \qquad (3)$$

where time zero corresponds to the system in H_2O buffer, a_i and τ_i are the amplitude and time constant of component *i*, respectively, and *m* is the number of components. Strictly speaking, each amino acid residue in the protein is characterized by an individual τ_i, implying that ideally *m* should equal the number of amino acid residues. But it is obviously impossible to determine several hundred parameters using a single experimental multiexponential curve. Therefore, two

Table 2: Amide I Frequencies of Most Typical Secondary Structural Elements in Proteins in H_2O and D_2O Environments[a]

secondary structure	frequency (cm^{-1}) H_2O	D_2O
α_I-helix	1658−1650	1655−1646
α_{II}-helix	1666−1658	1658−1652
3_{10}-helix	1670−1660	1670−1660
$\uparrow\downarrow\beta$-sheet	1638−1632	1636−1630
$\uparrow\downarrow\beta$-sheet	1695−1675[b]	1680−1670[b]
intermolecular β-sheet	1625−1615	1625−1615
β-turns	1685−1655	1675−1640
γ-turns	1690−1650	1690−1650
irregular	1660−1652	1648−1640
amide or aromatic side chains	1618−1605	1615−1600

[a] Data are taken from refs *27*, *30*, and *32*. [b] In an antiparallel β-sheet, a weaker band appears at higher frequencies in addition to the main component due to transition dipole coupling (*27*).

to four components are usually used to describe protein HX data (*21*, *23*, *33*, *53*). Since the HX kinetics reflect solvent accessibility and the strength of H-bonding in the protein, this implies that all protein residues can usually be divided into a small number of populations with similar dynamic properties.

For peripheral proteins such as PLA_2, which are not protected from the solvent by insertion into the membrane, the intensity of the amide II band at ~1545 cm^{-1} may nearly vanish shortly after exposure to D_2O. This makes it difficult to gain complete information about HX using the amide II band, including the slow component of exchange. In such cases, the H−D exchange kinetics can be determined using the amide I band, as described in the Supporting Information (see also refs *35* and *41*).

Gibbs free energies of HX (ΔG_{HX}) for each kinetic population have been determined and interpreted in terms of the structural features of corresponding residues (*33*, *53*).

$$\Delta G_{HX,i} = -RT \ln(\tau_0/\tau_i) \quad (4)$$

where τ_0 (0.487 s) is the time constant of HX for an unordered, solvent-exposed residue at 20 °C and pH* 7.0 (pD 7.4). For example, in the KcsA K^+ channel, three populations were identified; one was HX-resistant, while the other two were characterized by ΔG_{HX} values of 2.8 and 5.7 kcal/mol (*33*). Because 2.8 kcal/mol is similar to the ΔG of amide H-bonding, this population was suggested to comprise H-bonded α-helical residues lining the water-filled pore. The residues undergoing slow exchange were ascribed to partially solvent-accessible secondary structures, such as lipid-exposed transmembrane helices. Analysis of amide HX of co-reconstituted sarcoplasmic reticulum (SR) Ca^{2+}-ATPase and ^{13}C-labeled phospholamban (PLB), an integral regulatory protein, provided evidence for stabilization of α-helices within the Ca^{2+}-ATPase upon interaction with PLB (*53*).

Protein Secondary Structure. Determination of protein secondary structure by FTIR relies on the fact that the amide I vibrations of different secondary structures occur at different frequencies, as specified in Table 2. These are not strictly fixed frequencies, however. The frequencies generated by the same secondary structural element in different proteins are likely to vary within a narrow range due to differences in such factors as H-bonding strength and microenvironment

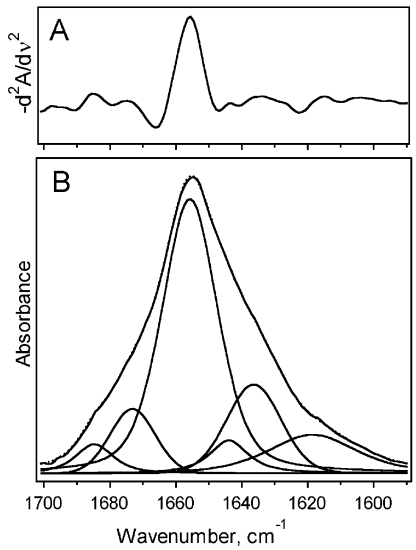

FIGURE 5: Results of curve fitting of the amide I band of *S. lividans* K^+ channel. The polarization-independent spectrum, shown in panel B, was obtained using the parallel and perpendicular spectra of Figure 4, corresponding to 2−10 min in D_2O ($A = A_{||} + 0.8A_{\perp}$). Six amide I components, shown in panel B, were found by curve fitting, using the frequencies identified by the second-derivative spectrum (panel A). The dotted line in panel B is the sum of all components.

Table 3: Secondary Structure Characterizaton of *S. lividans* K^+ Channel by ATR-FTIR Spectroscopy[a]

frequency of amide I component (cm^{-1})	assignment	fraction (%)
1684.8	turn or $\uparrow\downarrow\beta$-sheet	4.2
1673.2	turn or $\uparrow\downarrow\beta$-sheet	9.4
1655.8	α-helix	53.9
1643.9	irregular	5.3
1636.4	β-sheet	15.7
1618.6	side chains or intermolecular β-sheet	11.5

[a] The curve fitting data are shown in Figure 5.

("fingerprint" frequencies). Also, there are considerable overlaps between certain structural elements, especially in the region of 1700−1650 cm^{-1}, where various modes of β- and γ-turns overlap with the high-frequency counterpart of the antiparallel β-sheet and even with the α-helical component. The problem can be partially solved with the following procedure. Using the extinction coefficients for the low- and high-frequency components of the antiparallel β-sheet (7.6×10^7 and 5×10^6 cm/mol, respectively), one can determine the total antiparallel β-sheet fraction ($\uparrow\downarrow\beta_{total}$) to be $1.07f_{low}$, where f_{low} is the fraction of the low-frequency component (at ~1635 cm^{-1}) that usually does not overlap with other components. Then, the total turn fraction can be corrected by subtracting $0.07f_{low}$ from the fraction of components in the region of 1700−1660 cm^{-1}.

The structure of KcsA has been studied by ATR-FTIR (*33*). The second derivative of the amide I spectrum of KcsA (Figure 5A) exhibited a major α-helical component around 1655 cm^{-1}, and five weaker components. All six components were identified by a curve fitting program (Figure 5B) and were assigned to certain secondary structures, as shown in Table 3. The fractions of the areas of all components with respect to the whole amide I area roughly represent the fractions of corresponding secondary structures in the protein.

The crystal structure of the truncated KcsA (residues 23−119) contained 41% α-helix and no β-structure (*59*), while Table 3 reports 54% α-helix and ∼16% β-structure. It is possible that the fragment of the protein omitted in $KcsA_{23-119}$ incorporates both α-helical and β structures. This was indeed confirmed by the results of spin-label EPR studies on the full-length protein reconstituted in lipid membranes (*60*).

Orientation of Membrane Proteins. Membrane proteins form unique complexes with membrane lipids with the precise, functionally productive spatial orientation of the protein relative to the membrane plane (*61*−*64*). Orientations of both membrane-binding proteins and peptides can be determined by polarized ATR-FTIR spectroscopy. For polypeptides containing a single α-helix (or helices that are strictly parallel or antiparallel to each other), one has to evaluate the α-helical amide I ATR dichroic ratio [$R_\alpha^{ATR} = R^{ATR}(f_{\alpha||}/f_{\alpha\perp})$, where R^{ATR} ($A_{||}/A_\perp$) is the overall amide I dichroic ratio, and $f_{\alpha||}$ and $f_{\alpha\perp}$ are the α-helical fractions of the amide I band at parallel and perpendicular polarizations, respectively]. R_α^{ATR} is directly used to calculate the order parameter and the average tilt angle of the helix with eqs 1 and 3 of the Supporting Information. For a peptide that, in addition to α-helix, contains irregular (random) structure, the following expression may be used to evaluate R_α^{ATR}:

$$R_\alpha^{ATR} = \frac{R^{ATR}}{f_{\alpha\perp}} - R_{iso}\frac{1 - f_{\alpha\perp}}{f_{\alpha\perp}} \quad (5)$$

where R_{iso} [$=(E_x^2 + E_z^2)/E_y^2$] is the dichroic ratio of an isotropic sample, so evaluation of R_α^{ATR} requires accurate determination of only $f_{\alpha\perp}$. Procedures for finding R_α^{ATR} for peptides containing additional structures, such as β structure, are described in the Supporting Information.

Often, the orientations of α-helical segments of membrane-bound peptides or proteins are evaluated by ATR-FTIR either by using the total dichroic ratio of the amide I band (*47*, *50*, *51*) or by dividing the overall order parameter by the α-helical fraction of the molecule (*65*, *66*). The first approach may involve ambiguity due to contributions of non-α-helical structures in the measured dichroism, while the second approach is likely to involve large errors. For example, if the peptide contains an α-helical segment that is tilted toward the membrane surface and has a negative order parameter, but the overall order parameter is positive due to the other structures in the peptide, then division of the overall order parameter by the α-helical fraction will incorrectly indicate an upright helical orientation.

For proteins with differently oriented helices, the interpretation of R_α^{ATR} is complicated. Nevertheless, R_α^{ATR} was measured for rhodopsin using the α-helical components of the amide I band at different polarizations and was used to estimate the average orientation of helices (*67*). The average orientation of the transmembrane helices of bacteriorhodopsin (BR) was estimated by ascribing the measured overall dichroism to these helices (*51*, *68*, *69*). In the latter case, it is assumed that non-α-helical structures do not contribute to the observed dichroism, which is not necessarily plausible. Also, all helices are assumed to have similar orientations, whereas in both rhodopsin and BR, interhelical angles reach 25° (*70*, *71*).

A number of procedures have been offered that allow relatively reliable determination of the orientation of membrane-bound proteins. In the case of PLB, which has a transmembrane α-helix and a tilted cytoplasmic α-helix (*72*), the dichroic ratios of the transmembrane helix and of the full-length protein were measured independently, which allowed determination of the orientations of both helices (*39*). The orientation of a membrane-bound peripheral protein was estimated by fitting the experimental value of R_α^{ATR} with that obtained by positioning the crystal structure of the protein at the membrane surface (*44*). Orientation of a β-barrel protein in membranes was determined by combination of ATR dichroic ratios with tilt angles of strands relative to the barrel axis deduced from the high-resolution structure (*73*). The orientations of the transition dipole moments of various vibrational modes relative to transmembrane helices of BR were determined by combining dichroic ratios with the atomic-resolution structure of the protein (*74*). These latter studies demonstrate the advantage of using atomic structures of proteins to interpret ATR-FTIR data.

Isotope-Edited FTIR Spectroscopy

The vibrational frequency of a molecule composed of two atoms with masses m_1 and m_2 can be expressed as

$$\nu = \frac{1}{2\pi}\sqrt{k\left(\frac{1}{m_1} + \frac{1}{m_2}\right)} \quad (6)$$

where k is the bond strength. The frequency shift resulting from isotope substitutions has been used to study local and global structures of both proteins and lipids by "isotope-edited" FTIR spectroscopy (*75*). Analysis of FTIR spectra of phospholipids with selectively ^{13}C-labeled carbonyl groups suggested that the components of the carbonyl stretching band at ∼1742 or ∼1728 cm^{-1} were generated by C═O groups that were dehydrated or H-bonded to water, respectively (*76*, *77*); H-bonding of the carbonyl oxygen weakens the covalent C═O bond and decreases its vibrational frequency. The temperature dependence of spectra of lipids with unlabeled and deuterated hydrocarbon chains identified segregated lipid domains in membranes (*78*−*80*) and revealed selective interactions of membrane proteins with specific lipid components in membranes (*81*, *82*).

Because ^{13}C labeling of carbonyl groups of proteins substantially shifts the amide I band to lower frequencies, both uniform and site-specific ^{13}C (or ^{13}C and ^{15}N) labeling have been used in conformational analyses of proteins. Uniform labeling of one of two interacting proteins, such as a chaperone and its substrate proteins (*83*), receptors and ligands (*84*, *85*), calmodulin and target peptides (*86*), or bacterial transporters (*87*), has allowed detection of individual structural changes in both molecules via analysis of their spectrally separated amide I bands.

A major advantage of isotope-edited FTIR spectroscopy is that site-specific structures can be probed without a need for perturbing modifications such as mutagenesis or attachment of bulky molecular probes. Tadesse et al. (*88*) used synthetic peptides in which five consecutive residues were labeled with ^{13}C, resulting in an ∼36 cm^{-1} downshift of the amide I frequency and thus providing local structural information. This strategy has been used to determine the structures of specific sites in water-soluble and membrane-binding peptides (*58*, *89*−*93*).

Local structures in peptides and full-length proteins have been analyzed by labeling a single residue, or two residues, in the polypeptide chain. Rothschild and co-workers (*94*−*96*) developed a protein engineering technique that permitted incorporation of isotopically modified amino acids into selected sites of proteins. FTIR studies on BR, in which the backbone carbonyl carbons or side chain (ring) hydrogens of single tyrosines were labeled with ^{13}C or ^{2}H, respectively, identified residues that undergo structural changes upon functional transitions of the molecule. Labeling of just one residue in transmembrane peptides of PLB or glycophorin resulted in a new amide I component that was downshifted by 42−44 cm^{-1} and was assigned to the amide I band of the labeled amino acid (*47*, *97*). The frequency and dichroism of the shifted component were used to evaluate the local secondary structure, as well as the tilt angle and rotational orientation of peptides (*47*, *48*, *97*, *98*). Double $^{13}C{=}^{18}O$ labeling of a single residue has been used to move the labeled signal farther away from the main amide I band (from ∼1659 to ∼1595 cm^{-1}) and thus increase the spectral resolution (*99*). Finally, the CD_2 stretching modes of a single, C_α-deuterated glycine residue in a helical transmembrane peptide were used to determine the helix tilt and rotational orientation in supported membranes (*100*).

The results of isotope-edited FTIR when one or two residues are labeled in the polypeptide chain should be interpreted with caution. In such cases, delocalized vibrational modes, such as amide I or amide II bands, cannot be used to gain information about the local structure because these modes are contaminated with neighboring unlabeled residues. Labeling of segments, e.g., 5−10 consecutive residues, would provide more reliable information about the secondary structure and orientation of the segment, because in this case the contributions from the unlabeled residues will be minimized. In this respect, localized vibrational modes, such as backbone or side chain CD_2 stretching vibrations (*94*, *95*, *100*), may be interpreted in a more straightforward way than delocalized vibrational modes such as amide I or amide II.

Interfacial Enzymology

ATR-FTIR spectroscopy was used to measure activities of membrane-binding enzymes, such as PLA_2 (*34*, *35*) and triglycerol lipase (*101*), by monitoring the enzyme concentration-dependent decrease in the lipid signal. The use of membranes composed of an unlabeled acidic lipid (DPPG) and an acyl chain-deuterated zwitterionic lipid [DP(d_{62})PC] as substrates for PLA_2 indicated equal activity of the enzyme for both lipids (Figure 6), implying that increased activity of PLA_2 for negatively charged membranes results from stronger membrane−enzyme electrostatic interactions rather than selective hydrolysis of the acidic lipid (*34*). On the other hand, studies on PLA_2 activity against membranes composed of a lipid with one unlabeled and one deuterated acyl chain demonstrated that lipid hydrolysis is followed by preferential removal of the liberated lysolipid and accumulation of the free fatty acid in membranes (*34*).

Protein−Protein Interactions in Membranes

Isotope-edited ATR-FTIR spectroscopy has recently been used to study interactions between integral membrane proteins (*53*). Co-reconstitution of SR Ca^{2+}-ATPase with uniformly ^{13}C-labeled PLB permitted spectral resolution of both amide I and amide II bands of both proteins (Figure 7). Analysis of the spectra indicated that the inhibitory action of PLB involves stabilization of the α-helices within the Ca^{2+}-ATPase. This was confirmed by the PLB concentration-dependent increase in the fraction of HX-resistant residues in the Ca^{2+}-ATPase. Moreover, this latter dependence, in conjunction with measured Ca^{2+}-ATPase/PLB molar ratios, allowed quantitative characterization of the interaction between the two proteins with a binding constant of 7.1×10^4 M^{-1}. This binding constant was similar to that deduced from the inhibitory action of PLB on the Ca^{2+}-ATPase,

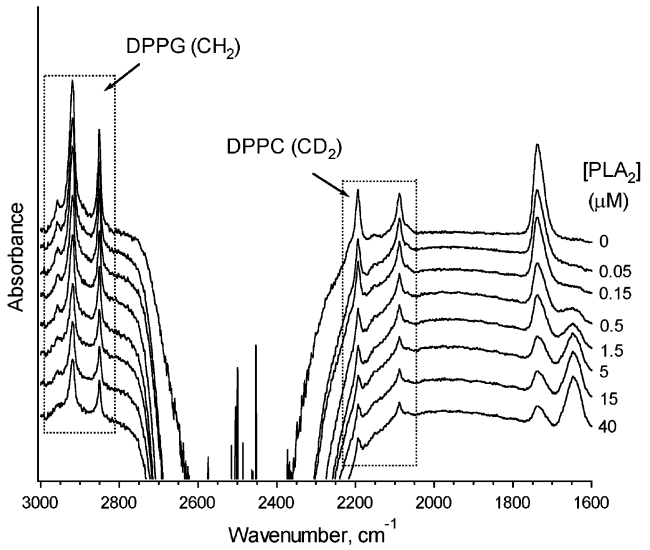

FIGURE 6: ATR-FTIR spectra of a supported membrane composed of an equimolar mixture of DPPG and DP(d_{62})PC as a function of PLA_2 concentration in the presence of 2 mM $CaCl_2$, 100 mM NaCl, 15 mM KCl, 1 mM NaN_3, and 10 mM Hepes in D_2O (pD 8.0). Dependencies of CH_2 stretching bands of DPPG and CD_2 stretching bands of DPPC (framed by dotted rectangles) on PLA_2 concentration were used to assess the selective hydrolysis of the acidic (DPPG) and zwitterionic (DPPC) lipids by PLA_2.

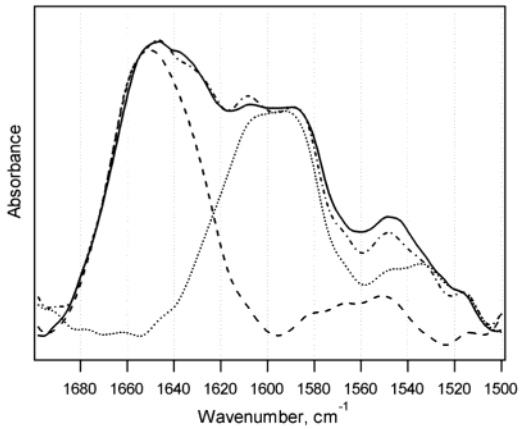

FIGURE 7: ATR-FTIR spectra of the Ca^{2+}-ATPase (- - -), of [^{13}C]-PLB (···), and following co-reconstitution of the Ca^{2+}-ATPase with an 11-fold molar excess of [^{13}C]PLB (—) and the sum of the individual spectra of the Ca^{2+}-ATPase and [^{13}C]PLB (-·-). The amide I and amide II bands of the Ca^{2+}-ATPase are at ∼1658 and ∼1546 cm^{-1}, respectively. Labeling of PLB with ^{13}C results in a shift of both amide I and amide II bands to 1608−1585 and ∼1525 cm^{-1}, respectively. These spectral separations allow analysis of structural changes in both proteins resulting from their interaction.

supporting the conclusion that the observed rigidification of the helical structures in the Ca^{2+}-ATPase by PLB was involved in the regulatory function of PLB.

Time-Resolved Difference Spectroscopy

Steady-state and time-resolved difference FTIR spectroscopy has been used in both direct transmission and ATR modes to determine light- or ligand-induced dynamic structural changes in membrane proteins. Spectral differences between the ground and activated states of proteins allow identification of structural units involved in functional transitions and characterization of underlying conformational changes (*102*−*106*). The time scale of typical vibrational modes in mid-infrared spectroscopy (e.g., $\sim 2 \times 10^{-14}$ s in the amide I region) allows measurements of fast conformational changes in proteins with picosecond to femtosecond time resolutions. Fast events in proteins have been detected by rapid-scan FTIR spectrsocopy, which is limited by the velocity of the mobile mirror and provides time resolutions of ∼10−100 ms, or step-scan spectroscopy, which records time-dependent changes in given absorbance bands at many fixed wavenumbers and then combines them to produce spectra with time resolutions on a time scale between microseconds and picoseconds (*107*−*111*). Time-resolved difference spectroscopy, i.e., analysis of fast spectral changes within regions that are assigned to certain structural and functional groups of proteins, has provided insight into the molecular details of several membrane proteins, including (bacterio)rhodopsin (*107*, *111*−*120*), different isoforms of cytochrome oxidases (*121*−*125*), photosynthetic reaction centers (*126*−*129*), SR Ca^{2+}-ATPase (*130*−*132*), and members of the Ras superfamily (*133*, *134*).

Simultaneous assessments of light-induced protonation and deprotonation of aspartic acid residues of BR, backbone motion of the protein, and retinal isomerization by rapid-scan FTIR at 7 ms resolution suggested a synchronized mechanism for light-driven proton transfer (*107*), and key Asp residues have been identified by site-directed mutagenesis (*135*, *136*). This model was later confirmed by atomic-resolution structures of wild-type and mutant BR (*6*, *137*, *138*). In a recent time-resolved difference FTIR study, the light-triggered electron and proton transfer reactions in a 100 kDa photosynthetic protein were monitored in a time frame ranging from 30 ns to 35 s, which provided unprecedented insight into the dynamic mechanism of electron and proton coupling that can hardly be obtained with other techniques (*129*).

Time-resolved difference ATR-FTIR spectroscopy offers a number of potential advantages compared to the transmission FTIR technique. In the ATR mode, conditions such as pH and reactants can be manipulated by means of perfusion without perturbation of the protein sample, and fast orientational changes of certain protein segments can be identified by recording time-resolved spectra at different polarizations of the incident light. Indeed, step-scan ATR-FTIR difference spectroscopy enabled characterization of fast ligand binding and redox reactions in cytochrome *c* oxidase (*121*) and transient changes in the p*K* values of single amino acid residues of BR involved in active proton transport (*112*, *113*). In case of thick layers of protein/lipid samples ($d \gg d_p$), spectra must be corrected for increased band intensities toward lower frequencies due to deeper penetration of the evanescent field into the sample (see eq 2 of the Supporting Information and ref *105*).

The orientation of membrane proteins and their structural elements can also be determined by direct transmission of polarized light through oriented samples that are positioned at different angles with respect to the plane of polarization. This technique has been used to determine the orientation of the transmembrane helices, individual carboxylic side chains, and the retinal chromophore of BR (*68*, *139*−*142*), as well as to gain structural information about other proteins and peptides (*143*, *144*). Polarized FTIR was used in the rapid-scan mode to determine changes in orientations of functionally important units of BR during the photocycle with a millisecond time resolution (*145*). This latter study, together with other time-resolved FTIR investigations where transient intermediate states of proteins were identified at superior time resolutions (*111*, *129*, *146*), demonstrates that polarized and time-resolved FTIR spectroscopy can provide invaluable insight into the molecular details of protein function that is out of reach of many other techniques.

Conclusions and Future Directions

ATR-FTIR spectroscopy is a powerful technique that is making inroads in the field of membrane biophysics and has already helped elucidate various aspects of the structure and function of membrane proteins and lipids. Often, protein/lipid samples for ATR-FTIR (*21*−*23*, *47*−*51*) or transmission FTIR experiments (*68*, *69*, *139*−*141*, *143*, *144*) are prepared by drying the sample on the surface of the internal reflection element or the FTIR window. Although in some cases the protein seems to maintain its functionality under these conditions (*21*, *23*), the absence of excess water is likely to affect the structure and function of both the protein and the lipid (*147*−*149*). Therefore, samples under bulk aqueous phase are more physiologically relevant than dry samples. Also, samples thicker than the depth of penetration of the evanescent field yield spectra in which absorbance intensity linearly increases with decreasing frequencies (*51*, *105*, *106*); this must be taken into account in data analysis.

Caution should be used in interpreting experimental data in terms of local or global secondary structure and orientation of proteins. Polarized spectra cannot be used for secondary structure determination, and delocalized vibrational modes (such as amide I) generated by single isotope-labeled residues cannot provide correct information about local structure or orientation. Segmental isotope labeling of proteins, which can be achieved using peptide ligation techniques (*150*), is an especially promising strategy for various purposes, such as determination of local structure and orientation of selected segments of proteins and for positioning of proteins on the membrane surface. The latter can be done by measuring the total α-helical dichroic ratio of the protein and that of a particular, isotope-labeled α-helix in the context of the whole protein. These two dichroic ratios can be used to determine the three-dimensional orientation of the membrane-bound protein.

SUPPORTING INFORMATION AVAILABLE

ATR-FTIR determination of order parameters and surface densities of membrane lipids and proteins, and measure-

ment of hydrogen exchange using the amide I band. This material is available free of charge via the Internet at http://pubs.acs.org.

REFERENCES

1. Rigaud, J.-L., Chami, M., Lambert, O., Levy, D., and Ranck, J.-L. (2000) *Biochim. Biophys. Acta 1508*, 112−128.
2. Garavito, R. M., and Ferguson-Miller, S. (2001) *J. Biol. Chem. 276*, 32403−32406.
3. Faham, S., and Bowie, J. U. (2002) *J. Mol. Biol. 316*, 1−6.
4. Pebay-Peyroula, E., Rummel, G., Rosenbusch, J. P., and Landau, E. M. (1997) *Science 277*, 1676−1681.
5. Belrhali, H., Nollert, P., Royant, A., Menzel, C., Rosenbusch, J. P., Landau, E. M., and Pebay-Peyroula, E. (1999) *Struct. Folding Des. 7*, 909−917.
6. Luecke, H., Schobert, B., Richter, H.-T., Cartailler, J.-P., and Lanyi, J. K. (1999) *J. Mol. Biol. 291*, 899−911.
7. Kolbe, M., Besir, H., Essen, L. O., and Oesterhalt, D. (2000) *Science 288*, 1390−1396.
8. Rouhani, S., Cartailler, J. P., Facciotti, M. T., Walian, P., Needleman, R., Lanyi, J. K., Glaeser, R. M., and Luecke, H. (2001) *J. Mol. Biol. 313*, 615−628.
9. Xu, R. X., Pawelczyk, T., Xia, T. H., and Brown, S. C. (1997) *Biochemistry 36*, 10709−10717.
10. Marassi, F. M., and Opella, S. J. (1998) *Curr. Opin. Struct. Biol. 8*, 640−648.
11. Opella, S. J., Nevzorov, A., Mesleb, M. F., and Marassi, F. M. (2002) *Biochem. Cell Biol. 80*, 597−604.
12. Cushley, R. J., and Okon, M. (2002) *Annu. Rev. Biophys. Biomol. Struct. 31*, 177−206.
13. Rosenbusch, J. P., Lustig, A., Grabo, M., Zulauf, M., and Regenass, M. (2001) *Micron 32*, 75−90.
14. Bowie, J. U. (2001) *Curr. Opin. Struct. Biol. 4*, 397−402.
15. Lee, A. G. (1998) *Biochim. Biophys. Acta 1376*, 381−390.
16. Killian, J. A., and von Heijne, G. (2000) *Trends Biochem. Sci. 25*, 429−434.
17. White, S. H., Ladokhin, A. S., Jayasinghe, S., and Hristova, K. (2001) *J. Biol. Chem. 276*, 32395−32398.
18. Fringeli, U. P. (1993) in *Internal Reflection Spectroscopy* (Mirabella, F. M., Jr., Ed.) pp 255−324, Marcel Dekker, New York.
19. Axelsen, P. H., and Citra, M. J. (1996) *Prog. Biophys. Mol. Biol. 66*, 227−253.
20. Tamm, L. K., and Tatulian, S. A. (1997) *Q. Rev. Biophys. 30*, 365−429.
21. Goormaghtigh, E., Raussens, V., and Ruysschaert, J.-M. (1999) *Biochim. Biophys. Acta 1422*, 105−185.
22. Vigano, C., Manciu, L., Buyse, F., Goormaghtigh, E., and Ruysschaert, J.-M. (2000) *Biopolymers 55*, 373−380.
23. Vigano, C., Goormaghtigh, E., and Ruysschaert, J.-M. (2003) *Chem. Phys. Lipids 122*, 121−135.
24. Marsh, D. (1998) *Biophys. J. 75*, 354−358.
25. Marsh, D. (1999) *Biophys. J. 77*, 2630−2637.
26. Marsh, D., Müller, M., and Schmitt, F.-J. (2000) *Biophys. J. 78*, 2499−2510.
27. Krimm, S., and Bandekar, J. (1986) *Adv. Protein Chem. 38*, 181−364.
28. Mendelsohn, R., and Mantsch, H. H. (1986) in *Progress in Protein−Lipid Interactions* (Watts, A., and De Pont, J. J. H. H. M., Eds.) pp 103−146, Elsevier, Amsterdam.
29. Surewicz, W. K., Mantsch, H. H., and Chapman, D. (1993) *Biochemistry 32*, 389−394.
30. Arrondo, J. L. R., Muga, A., Castresana, J., and Goñi, F. M. (1993) *Prog. Biophys. Mol. Biol. 59*, 23−56.
31. Haris, P. I., and Chapman, D. (1995) *Biopolymers 37*, 251−263.
32. Arrondo, J. L. R., and Goñi, F. M. (1999) *Prog. Biophys. Mol. Biol. 72*, 367−405.
33. Tatulian, S. A., Cortes, D. M., and Perozo, E. (1998) *FEBS Lett. 423*, 205−212.
34. Tatulian, S. A. (2001) *Biophys. J. 80*, 789−800.
35. Tatulian, S. A. (2003) *Biophys. J. 84*, 1773−1783.
36. Sackmann, E. (1996) *Science 271*, 43−48.
37. Seitz, M., Ter-Ovanesyan, E., Hausch, M., Park, C. K., Zasadzinski, J. A., Zental, R., and Israelachvili, J. N. (2000) *Langmuir 16*, 6067−6070.
38. Nollert, P., Kiefer, H., and Jähnig, F. (1995) *Biophys. J. 69*, 1447−1455.
39. Tatulian, S. A., Jones, L. R., Reddy, L. G., Stokes, D. L., and Tamm, L. K. (1995) *Biochemistry 34*, 4448−4456.
40. Tatulian, S. A., Hinterdorfer, P., Baber, G., and Tamm, L. K. (1995) *EMBO J. 14*, 5514−5523.
41. Tatulian, S. A., Biltonen, R. L., and Tamm, L. K. (1997) *J. Mol. Biol. 268*, 809−815.
42. Majewski, J., Wong, J. Y., Park, C. K., Seitz, M., Israelachvili, J. N., and Smith, G. S. (1998) *Biophys. J. 75*, 2363−2367.
43. Plant, A. L. (1999) *Langmuir 15*, 5128−5135.
44. Silvestro, L., and Axelsen, P. H. (1999) *Biochemistry 38*, 113−121.
45. Wong, J. Y., Park, C. K., Seitz, M., and Israelachvili, J. N. (1999) *Biophys. J. 77*, 1458−1468.
46. Johnson, J. M., Ha, T., Chu, S., and Boxer, G. (2002) *Biophys. J. 83*, 3371−3379.
47. Arkin, I. T., MacKenzie, K. R., and Brünger, A. T. (1997) *J. Am. Chem. Soc. 119*, 8973−8980.
48. Kukol, A., and Arkin, I. (1999) *Biophys. J. 77*, 1594−1601.
49. Abrecht, H., Goormaghtigh, E., Ruysschaert, J.-M., and Homblé, F. (2000) *J. Biol. Chem. 275*, 40992−40999.
50. Chia, C. S. B., Torres, J., Cooper, M. A., Arkin, I. T., and Bowie, J. H. (2002) *FEBS Lett. 512*, 47−51.
51. Smith, S. O., Eilers, M., Song, D., Crocker, E., Ying, W., Groesbeek, M., Metz, G., Ziliox, M., and Aimoto, S. (2002) *Biophys. J. 82*, 2476−2486.
52. Tatulian, S. A., Stezcko, J., and Minor, W. (1998) *Biochemistry 37*, 15481−15490.
53. Tatulian, S. A., Chen, B., Li, J., Negash, S., Middaugh, C. R., Bigelow, D. J., and Squier, T. C. (2002) *Biochemistry 41*, 741−751.
54. Mantsch, H. H., and McElhaney, R. N. (1991) *Chem. Phys. Lipids 57*, 213−226.
55. Fringeli, U. P., Apell, H.-J., Fringeli, M., and Läuger, P. (1989) *Biochim. Biophys. Acta 984*, 301−312.
56. Fringeli, U. P., and Günthard, H. H. (1981) in *Membrane Spectroscopy* (Grell, E., Ed.) pp 270−332, Springer-Verlag, Berlin.
57. Venyaminov, S. Y., and Kalnin, N. N. (1990) *Biopolymers 30*, 1259−1271.
58. Tatulian, S. A., and Tamm, L. K. (2000) *Biochemistry 39*, 496−507.
59. Doyle, D. A., Cabral, J. M., Pfuetzner, R. A., Kuo, A., Gulbis, J. M., Cohen, S. L., Chait, B. T., and MacKinnon, R. (1998) *Science 280*, 69−77.
60. Cortes, M. D., Guello, L. G., and Perozo, E. (2001) *J. Gen. Physiol. 117*, 165−180.
61. Ball, A., Nielsen, R., Gelb, M. H., and Robinson, B. H. (1999) *Proc. Natl. Acad. Sci. U.S.A. 96*, 6637−6642.
62. Lin, Y., Nielsen, R., Murray, D., Hubbell, W. L., Meiler, C., Robinson, B. H., and Gelb, M. H. (1998) *Science 279*, 1925−1929.
63. Spencer, R. H., and Rees, D. C. (2002) *Annu. Rev. Biophys. Biomol. Struct. 31*, 207−233.
64. Frazier, A. A., Roller, C. R., Havelka, J. J., Hinderliter, A., and Cafiso, D. S. (2003) *Biochemistry 42*, 96−105.
65. Frey, S., and Tamm, L. K. (1991) *Biophys. J. 60*, 922−930.
66. Gray, C., and Tamm, L. K. (1998) *Protein Sci. 7*, 2359−2373.
67. Michel-Villaz, M., Saibil, H. R., and Charbe, M. (1979) *Proc. Natl. Acad. Sci. U.S.A. 76*, 4405−4408.
68. Nabedryk, E., Bardin, A. M., and Breton, J. (1985) *Biophys. J. 48*, 873−876.
69. Nabedryk, E., and Breton, J. (1981) *Biochim. Biophys. Acta 635*, 515−524.
70. Grigorieff, N., Ceska, T. A., Downing, K. H., Baldwin, J. M., and Henderson, R. (1996) *J. Mol. Biol. 259*, 393−421.
71. Unger, V. M., Hargrave, P. A., Baldwin, J. M., and Schertler, G. F. X. (1997) *Nature 389*, 203−206.
72. Lamberth, S., Schmid, H., Muenchbach, M., Vorherr, T., Krebs, J., Carafoli, E., and Griesinger, C. (2000) *Helv. Chim. Acta 83*, 2141−2152.
73. Páli, T., and Marsh, D. (2001) *Biophys. J. 80*, 2789−2797.
74. Marsh, D., and Páli, T. (2001) *Biophys. J. 80*, 305−312.
75. Fabian, H., Chapman, D., and Mantsch, H. H. (1996) in *Infrared Spectroscopy of Biomolecules* (Mantsch, H. H., and Chapman, D., Eds.) pp 341−352, Wiley-Liss, New York.
76. Blume, A., Hübner, W., and Messner, G. (1988) *Biochemistry 27*, 8239−8249.
77. Hübner, W., Mantsch, H. H., Paltauf, F., and Hauser, H. (1994) *Biochemistry 33*, 320−326.

78. Mendelsohn, R., Liang, G. L., Strauss, H. L., and Snyder, R. G. (1995) *Biophys. J. 69*, 1987−1998.
79. Moore, D. J., Sills, R. H., and Mendelsohn, R. (1997) *Biochemistry 36*, 660−664.
80. Chen, H.-C., Mendelsohn, R., Rerek, M. E., and Moore, D. J. (2001) *Biochim. Biophys. Acta 1512*, 345−356.
81. Lasch, P., Schultz, C. P., and Neumann, D. (1998) *Biophys. J. 75*, 840−852.
82. Brockman, J. M., Wang, Z., Notter, R. H., and Dluhy, R. A. (2003) *Biophys. J. 84*, 326−340.
83. Das, K. P., Choo-Smith, L.-P., Petrash, J. M., and Surewicz, W. K. (1999) *J. Biol. Chem. 274*, 33209−33212.
84. Li, T., Horan, T., Osslund, T., Stearns, G., and Arakawa, T. (1997) *Biochemistry 36*, 8849−8857.
85. Li, T., Talvenheimo, J., Zeni, L., Rosenfeld, R., Stearns, G., and Arakawa, T. (2002) *Biopolymers 67*, 10−19.
86. Zhang, M., Fabian, H., Mantsch, H. H., and Vogel, H. J. (1994) *Biochemistry 33*, 10883−10888.
87. Haris, P. I., Robillard, G. T., van Dijk, A. A., and Chapman, D. (1992) *Biochemistry 31*, 6279−6284.
88. Tadesse, L., Nazarbeghi, R., and Walters, L. (1991) *J. Am. Chem. Soc. 113*, 7036−7037.
89. Gordon, L. M., Mobley, P. W., Pilpa, R., Sherman, M. A., and Waring, A. J. (2002) *Biochim. Biophys. Acta 1559*, 96−120.
90. Decatur, S. M. (2000) *Biopolymers 54*, 180−185.
91. Gangani, R. A., Silva, D., Nguyen, J. Y., and Decatur, S. M. (2002) *Biochemistry 41*, 15296−15303.
92. Venyaminov, S. Yu., Hedstrom, J. F., and Prendergast, F. G. (2001) *Proteins: Struct., Funct., Genet. 45*, 81−89.
93. Huang, C.-Y., Getahun, Z., Zhu, Y., Klemke, J. W., DeGrado, W. F., and Gai, F. (2002) *Proc. Natl. Acad. Sci. U.S.A. 99*, 2788−2793.
94. Sonar, S., Lee, C. P., Coleman, M., Patel, N., Liu, X., Marti, T., Khorana, H. G., RajBhandary, U. L., and Rothschild, K. J. (1994) *Nat. Struct. Biol. 1*, 495−496.
95. Liu, X.-M., Sonar, S., Lee, C.-P., Coleman, M., RajBhandary, U. L., and Rothschild, K. J. (1995) *Biophys. Chem. 56*, 63−70.
96. Ludlam, C. F. C., Sonar, S., Lee, C.-P., Coleman, M., Herzfeld, J., RajBhandary, U. L., and Rothschild, K. J. (1995) *Biochemistry 34*, 2−6.
97. Ludlam, C. F. C., Arkin, I. T., Liu, X. M., Rothman, M. S., Rath, P., Aimoto, S., Smith, S. O., Engelman, D. M., and Rothschild, K. J. (1996) *Biophys. J. 70*, 1728−1736.
98. Arkin, I. T., MacKenzie, K. R., Fisher, L., Aimoto, S., Engelman, D. M., and Smith, S. O. (1996) *Nat. Struct. Biol. 3*, 240−243.
99. Torres, J., Kukol, A., Goodman, J. M., and Arkin, I. T. (2001) *Biopolymers 59*, 396−401.
100. Torres, J., Kukol, A., and Arkin, I. T. (2000) *Biophys. J. 79*, 3139−3143.
101. Snabe, T., and Petersen, S. B. (2002) *J. Biotechnol. 95*, 145−155.
102. Nabedryk, E., Breton, J., Sebban, P., and Baciou, L. (2003) *Biochemistry 42*, 5819−5827.
103. Furutani, Y., Sudo, Y., Kamo, N., and Kandori, H. (2003) *Biochemistry 42*, 4837−4842.
104. Barth, A. (2002) *Biopolymers 67*, 237−241.
105. Rich, P. R., and Breton, J. (2002) *Biochemistry 41*, 967−973.
106. Iwaki, M., Breton, J., and Rich, P. R. (2002) *Biochim. Biophys. Acta 1555*, 116−121.
107. Gerwert, K., Souvignier, G., and Hess, B. (1990) *Proc. Natl. Acad. Sci. U.S.A. 87*, 9774−9778.
108. Johnson, T. J., Simon, A., Well, J. M., and Harris, G. W. (1993) *Appl. Spectrosc. 47*, 1376−1381.
109. Slayton, R. M., and Anfinrud, P. A. (1997) *Curr. Opin. Struct. Biol. 7*, 717−721.
110. Gerwert, K. (1999) *Biol. Chem. 380*, 931−935.
111. Herbst, J., Heyne, K., and Diller, R. (2002) *Science 297*, 822−825.
112. Zscherp, C., Schlesinger, R., and Heberle, J. (2001) *Biochem. Biophys. Res. Commun. 283*, 57−63.
113. Zscherp, C., Schlesinger, R., Tittor, J., Oesterhelt, D., and Heberle, J. (1999) *Proc. Natl. Acad. Sci. U.S.A. 96*, 5489−5503.
114. Wang, J., and El-Sayed, M. (2001) *Biophys. J. 80*, 961−971.
115. Hutson, M. S., Alexiev, U., Shilov, S. V., Wise, K. J., and Braiman, M. S. (2000) *Biochemistry 39*, 13189−13200.
116. Hein, M., Wegener, A. A., Engelhard, M., and Siebert, F. (2003) *Biophys. J. 84*, 1208−1217.
117. Dioumaev, A. K., Brown, L. S., Shih, J., Spudich, E. N., Spudich, J. L., and Lanyi, J. K. (2002) *Biochemistry 41*, 5348−5358.
118. Brown, L. S., Dioumaev, A. K., Lanyi, J. K., Spudich, E. N., and Spudich, J. L. (2001) *J. Biol. Chem. 276*, 32495−32505.
119. Hackmann, C., Guijarro, J., Chizhov, I., Engelhard, M., Rödig, C., and Siebert, F. (2001) *Biophys. J. 81*, 394−406.
120. Hutson, M. S., Shilov, S. V., Krebs, R., and Braiman, M. S. (2001) *Biophys. J. 80*, 1452−1465.
121. Nyquist, R. M., Heitbrink, D., Bolwien, C., Wells, T. A., Gennis, R. B., and Heberle, J. (2001) *FEBS Lett. 505*, 63−67.
122. Koutsoupakis, K., Stavrakis, S., Soulimane, T., and Varotsis, C. (2003) *J. Biol. Chem. 278*, 14893−14896.
123. Pinakoulaki, E., Soulimane, T., and Varotsis, C. (2002) *J. Biol. Chem. 277*, 32867−32874.
124. Bailey, J. A., Tomson, F. L., Mecklenburg, S. L., MacDonald, G. M., Katsonouri, A., Puustinen, A., Gennis, R. B., Woodruff, W. H., and Dyer, R. B. (2002) *Biochemistry 41*, 2675−2683.
125. Heitbrink, D., Sigurdson, H., Bolwien, C., Brzezinski, P., and Heberle, J. (2002) *Biophys. J. 82*, 1−10.
126. Mezzetti, A., Leibl, W., Breton, J., and Nabedryk, E. (2003) *FEBS Lett. 537*, 161−165.
127. Noguchi, T., Tomo, T., and Kato, C. (2001) *Biochemistry 40*, 2176−2185.
128. Alaya, I., Kim, S., and Barry, B. A. (1999) *Biophys. J. 77*, 2137−2144.
129. Remy, A., and Gerwert, K. (2003) *Nat. Struct. Biol. 10*, 637−644.
130. Barth, A. (1999) *J. Biol. Chem. 274*, 22170−22175.
131. Liu, M., and Barth, A. (2003) *J. Biol. Chem. 278*, 10112−10118.
132. Troullier, A., Gerwert, K., and Dupont, Y. (1996) *Biophys. J. 71*, 2970−2983.
133. Du, X., Frei, H., and Kim, S.-H. (2000) *J. Biol. Chem. 275*, 8492−8500.
134. Allin, C., and Gerwert, K. (2001) *Biochemistry 40*, 3037−3046.
135. Gerwert, K., Hess, B., Soppa, J., and Oesterhelt, D. (1989) *Proc. Natl. Acad. Sci. U.S.A. 86*, 4943−4947.
136. Braiman, M. S., Mogi, T., Marti, T., Stern, L. J., Khorana, H. G., and Rothschild, K. J. (1988) *Biochemistry 27*, 8516−8520.
137. Luecke, H., Schobert, B., Cartailler, J. P., Richter, H. T., Rosengarth, A., Needleman, R., and Lanyi, J. K. (2000) *J. Mol. Biol. 300*, 1237−1255.
138. Spassov, V. Z., Luecke, H., Gerwert, K., and Bashford, D. (2001) *J. Mol. Biol. 312*, 203−219.
139. Rothschild, K. J., and Clark, N. A. (1979) *Biophys. J. 25*, 473−487.
140. Earnest, T. N., Roepe, P., Braiman, M. S., and Rothschild, K. J. (1986) *Biochemistry 25*, 7793−7798.
141. Nabedryk, E., and Breton, J. (1986) *FEBS Lett. 202*, 356−360.
142. Kandori, H., Belenky, M., and Herzfeld, J. (2002) *Biochemistry 41*, 6026−6031.
143. Nabedryk, E., Gingold, M. P., and Breton, J. (1982) *Biophys. J. 38*, 243−249.
144. Nabedryk, E., Garavito, R. M., and Breton, J. (1988) *Biophys. J. 53*, 671−676.
145. Kelemen, L., and Ormos, P. (2001) *Biophys. J. 81*, 3577−3589.
146. Brudler, R., Rammelsberg, R., Woo, T. T., Getzoff, E. D., and Gerwert, K. (2001) *Nat. Struct. Biol. 8*, 265−270.
147. Wolkers, W. F., Looper, S. A., McKiernan, A. E., Tsvetkova, N. M., Tablin, F., and Crowe, J. H. (2002) *Mol. Membr. Biol. 19*, 201−210.
148. Goyal, K., Tisi, L., Basran, A., Browne, J., Burnell, A., Zurdo, J., and Tunnacliffe, A. (2003) *J. Biol. Chem. 278*, 12977−12984.
149. Conboy, J. C., Liu, S., O'Brien, D. F., and Saavedra, S. S. (2003) *Biomacromolecules 4*, 841−849.
150. Cowburn, D., and Muir, T. W. (2001) *Methods Enzymol. 339*, 41−54.

BI034235+